

# Observation of Van Hove singularities in twisted graphene layers

Guohong Li<sup>1</sup>, A. Luican<sup>1</sup>, J. M. B. Lopes dos Santos<sup>2</sup>, A. H. Castro Neto<sup>3</sup>, A. Reina<sup>4</sup>, J. Kong<sup>5</sup> and E. Y. Andrei<sup>1\*</sup>

**Electronic instabilities at the crossing of the Fermi energy with a Van Hove singularity<sup>1</sup> in the density of states often lead to new phases of matter such as superconductivity<sup>2,3</sup>, magnetism<sup>4</sup> or density waves<sup>5</sup>. However, in most materials this condition is difficult to control. In the case of single-layer graphene, the singularity is too far from the Fermi energy<sup>6</sup> and hence difficult to reach with standard doping and gating techniques<sup>7</sup>. Here we report the observation of low-energy Van Hove singularities in twisted graphene layers seen as two pronounced peaks in the density of states measured by scanning tunnelling spectroscopy. We demonstrate that a rotation between stacked graphene layers can generate Van Hove singularities, which can be brought arbitrarily close to the Fermi energy by varying the angle of rotation. This opens intriguing prospects for Van Hove singularity engineering of electronic phases.**

In two dimensions, a saddle point in the electronic band structure leads to a divergence in the density of states, also known as a Van Hove singularity<sup>1</sup> (VHS). When the Fermi energy ( $E_F$ ) is close to the VHS, interactions, however weak, are magnified by the enhanced density of states (DOS), resulting in instabilities, which can give rise to new phases of matter<sup>2–5</sup> with desirable properties. This implies the possibility of engineering material properties by bringing  $E_F$  and the VHS together. However, in most materials one cannot change the position of the VHS in the band structure. Instead, it may be possible to tune  $E_F$  through the VHS by chemical doping<sup>8</sup> or by gating<sup>7</sup>. In this regard, graphene, the recently discovered two-dimensional form of carbon, is quite special<sup>5,9</sup>. It has linearly dispersing bands at the K ( $K'$ ) point in the Brillouin zone, the so-called Dirac points, and a DOS that is linear and vanishes at Dirac point. The fact that this material is truly two-dimensional and has a low DOS means that it cannot screen applied electric fields, allowing for strong gating and ambipolar behaviour<sup>7</sup>. However, although the band structure of graphene<sup>5</sup> contains a VHS, its large distance from the Dirac point makes it prohibitively difficult to reach by either gating or chemical doping. We show that by introducing a rotation between stacked graphene layers, it is possible to induce VHSs that are within the range of  $E_F$  achievable by gate tuning. As the samples studied here are not intentionally doped,  $E_F$  is within a few millielectronvolts of the Dirac point.

Rotation between graphene layers is often observed as a Moiré pattern on graphite surfaces<sup>10</sup>, as illustrated in Fig. 1. Graphite consists of stacked layers of graphene, the lattice structure of which contains two interpenetrating triangular sublattices, denoted A and B. In the most common (Bernal) stacking, adjacent layers

are shifted by one atomic spacing, so that B atoms of layer 2 (B2) sit directly on top of A atoms of layer 1 (A1) and B1 and A2 atoms are in the centre of the hexagons of the opposing layer. Assuming a rotation through an angle  $\theta$  about an A1 (B2) site in bilayer graphene, a set of conditions for commensurate periodic structures leading to Moiré patterns is easily derived<sup>11</sup>  $\cos(\theta_i) = (3i^2 + 3i + 1/2)/(3i^2 + 3i + 1)$ , with  $i$  being an integer ( $i=0$ ,  $\theta = 60^\circ$  corresponds to AA stacking and  $i \rightarrow \infty$ ,  $\theta = 0^\circ$  to AB stacking) and lattice constant of the superlattice  $L = a_0 \sqrt{3i^2 + 3i + 1}$ , where  $a_0 \sim 2.46 \text{ \AA}$  is the atomic lattice constant. For the extended Moiré pattern in Fig. 1,  $\theta_i = 1.79^\circ$  is obtained from the superlattice period,  $L = 7.7 \pm 0.3 \text{ nm}$ , corresponding to  $i = 18$ .

Thus far, most work on Moiré patterns focused on structural aspects revealed by scanning tunnelling microscopy (STM), but their effect on the electronic properties has not been addressed. By using scanning tunnelling spectroscopy (STS), we find that rotation markedly alters the DOS. Figure 2 shows the tunnelling differential conductance,  $dI/dV$ , a quantity proportional to the local DOS (ref. 12). In regions inside the Moiré pattern (M1 and M2), the spectra develop two sharp peaks flanking the Dirac points with energy separation  $\Delta E_{\text{vhs}} \sim 82 \text{ meV}$ . Below, we show that these peaks correspond to rotation-induced VHSs. The effect of the VHS on the DOS is evident in the energy dependence of the  $dI/dV$  maps. Close to the VHS, the maps develop a strong density modulation (Figs 2f and 3c), characteristic of charge-density waves (CDWs), suggesting an impending Fermi-surface instability. In contrast, for energies away from the VHS, the charge density becomes nearly homogeneous.

To explore the angle dependence of  $\Delta E_{\text{vhs}}$ , we studied graphene layers prepared by chemical vapour deposition<sup>13</sup> (CVD). CVD graphene layers have a strong twisting tendency revealed by Moiré patterns with a range of rotation angles. The example in Fig. 3a shows a pattern, corresponding to  $\theta \sim 1.16^\circ$ . The STS spectra in this region reveal strong VHSs (Fig. 3b) with a much smaller  $\Delta E_{\text{vhs}} \sim 12 \text{ meV}$ . The pronounced spatial modulation of the  $dI/dV$  maps at energies close to these VHSs (Fig. 3c), indicating the formation of a CDW, is significantly stronger than for the pattern in Fig. 2f, where the more widely separated VHSs are farther away from the Fermi energy. For a pattern with an even larger angle,  $\theta \sim 3.4^\circ$ , and  $\Delta E_{\text{vhs}} \sim 430 \text{ meV}$ , the localization is weaker still (see Supplementary Fig. S3), consistent with theoretical predictions<sup>14</sup>.

We next show that the VHSs are induced by the rotation and use the model developed in ref. 11 to derive the angle dependence of  $\Delta E_{\text{vhs}}$ . A rotation between two graphene layers causes a shift between the corresponding Dirac points in momentum space, so

<sup>1</sup>Department of Physics and Astronomy, Rutgers University, Piscataway, New Jersey 08855, USA, <sup>2</sup>CFP and Departamento de Física, Faculdade de Ciências Universidade do Porto, 4169-007 Porto, Portugal, <sup>3</sup>Department of Physics, Boston University, 590 Commonwealth Avenue, Boston, Massachusetts 02215, USA, <sup>4</sup>Department of Materials Science and Engineering, MIT, Cambridge, Massachusetts 02139, USA, <sup>5</sup>Department of Electrical Engineering and Computer Science, MIT, Cambridge, Massachusetts 02139, USA. \*e-mail: eandrei@physics.rutgers.edu.

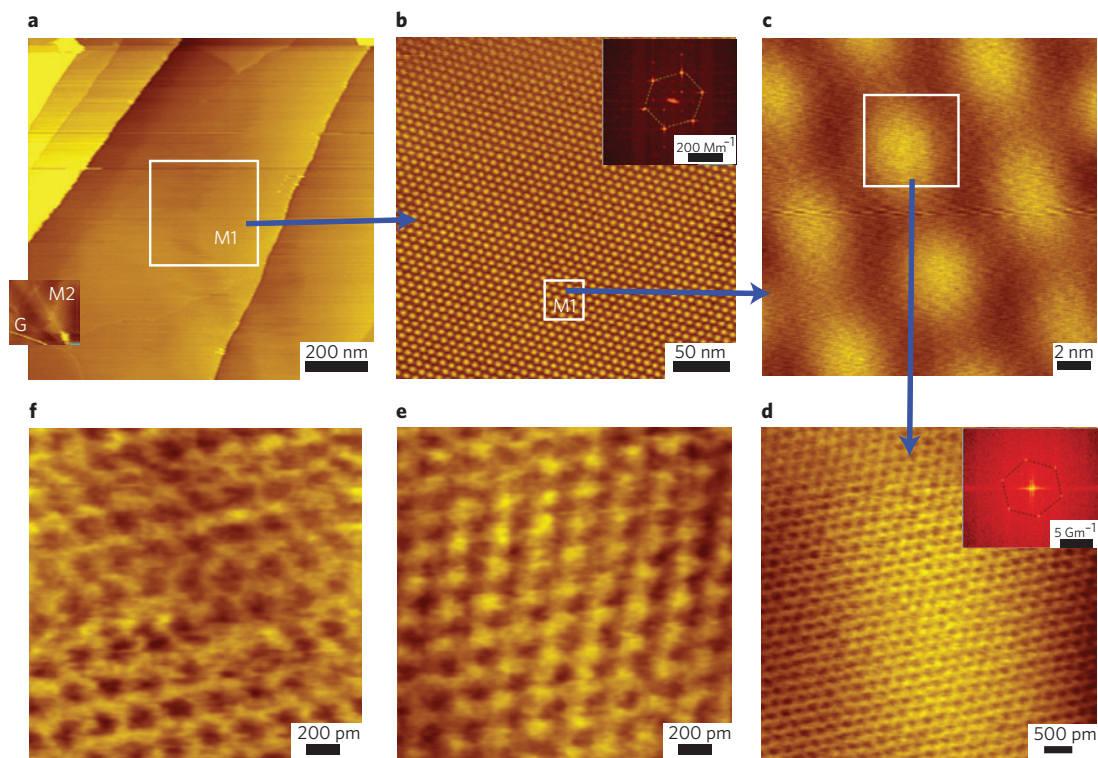


**Figure 1 | STM of a graphene flake on a freshly cleaved surface of highly oriented pyrolytic graphite revealing a Moiré pattern.** **a**, Large-area scan of a graphene flake. Regions M2 and G flank the boundary of the Moiré pattern. **b**, Zoom-in of the frame in **a**, showing a Moiré pattern with period  $7.7 \pm 0.3$  nm. Inset: Fourier transforms of the superstructure. **c**, Zoom-in to the centre of the pattern, region M1. **d**, Atomic-resolution image of a bright spot. Inset: Fourier transforms of the atomic-resolution image. **e, f**, Atomic-resolution image on bright and dark regions of the pattern, showing a well-ordered triangular lattice within the bright spots (**e**) and a less-ordered honeycomb-like structure in between (**f**). The former indicates Bernal-stacked layers<sup>16,23</sup>, whereas the latter suggests slipped stacking, resulting from a small-angle rotation between layers. Tunnelling current 20 pA, sample bias voltage 300 mV.

that the Dirac wavevector of the rotated layer is  $K^\theta = K + \Delta K$ , where  $\Delta K = K \times 2 \sin(\theta/2)$ . If we use the same origin of momentum for the two layers, so that a uniform hopping couples states of the same momentum in both layers, the zero-energy states do not occur at  $k = 0$ , but rather at  $k = -\Delta K/2$  in layer 1 and  $k = \Delta K/2$  in layer 2. Unlike in the AB stacked bilayer, there is no direct coupling of the zero-energy states of one layer to the zero-energy states of the other. As shown in ref. 11, the states near the Dirac cone of each layer couple with amplitudes of order  $t_\perp^\theta \approx 0.4 t_\perp$  to states of energy  $\pm \hbar v_F \Delta K$  of the opposing layer and the linear dispersion is preserved near zero energy. Here,  $t_\perp$  is the interlayer hopping for unrotated layers and  $v_F \sim 10^6$  m s<sup>-1</sup> is the Fermi velocity. The two Dirac cones intersect near the centre of the superlattice Brillouin zone and hybridize, resulting in a saddle point in the energy dispersion and in two symmetric VHSs (Fig. 4a).

This mechanism of rotation-induced low-energy VHSs is not restricted to the bilayer. We extended the calculation to a trilayer consisting of an AB stacked bilayer and a third rotated layer on top and again found two VHSs in the DOS (Fig. 4b). In both cases,  $\Delta E_{\text{vhs}}$  is controlled by the energy scale  $\hbar v_F \Delta K \propto \theta$ . Figure 4c shows that this model accounts well for the experimental angle dependence of  $\Delta E_{\text{vhs}}$ .

This analysis shows that the mechanism behind the formation of VHSs is quite robust, and we expect it to apply more generally whenever one layer is rotated with respect to the others, even for a graphene flake over graphite. The strong twisting-angle dependence of  $\Delta E_{\text{vhs}}$  is its unmistakable signature.

In the bilayer, the two Van Hove peaks are exactly symmetrical, whereas in the trilayer, a slight asymmetry occurs because of the third layer, but not as large as that observed experimentally. The discrepancy can be attributed to two factors. First, the experiments

probe the local DOS, which varies across the unit cell of the Moiré pattern, whereas the calculation refers to the total DOS. Averaging the data over several unit cells reduces the asymmetry. Second, a bias between the layers can also enhance the asymmetry. In the AB stacked bilayer, a perpendicular electric field opens a gap in the spectrum<sup>15</sup>; not so in the twisted bilayer. As states close to zero energy result from the hybridization of zero-energy states in one layer with states of energy  $\pm \hbar v_F \Delta K$  in the other, the corresponding wavefunctions have different weights in the two layers; when an electric field is applied, the two Dirac points move in opposite directions in energy<sup>11</sup>. The positive and negative energy states at the saddle points now have different weights in the two layers. As the STM probes predominantly the top layer, we expect this asymmetry in the STS. This effect of the bias in the DOS of the bilayer is shown in Fig. 4b (mid-panel).

It is important to note that the VHSs can form only in the presence of finite interlayer coupling. For vanishingly small interlayer coupling,  $t_\perp \sim 0$ , as is the case when a detached graphene flake is found on a graphite substrate<sup>16</sup> (see also Supplementary Information), the VHSs will not form even though a Moiré pattern may be visible in the STM images<sup>17</sup> (Supplementary Information). It is well known that on the surface of graphite one often finds graphene flakes loosely bound to the surface where interlayer coupling is completely suppressed<sup>16</sup>. Such flakes, regardless of the presence or absence of rotation with respect to the underlying layer, show an uninterrupted honeycomb structure and a Landau-level sequence characteristic of massless Dirac fermions<sup>16</sup>. However, they do not show VHSs in their zero-field DOS.

The situation here is reminiscent of transition-metal dichalcogenides<sup>14</sup>, which form triangular lattices where both CDWs and superconductivity are observed<sup>18</sup>. In fact, these materials have

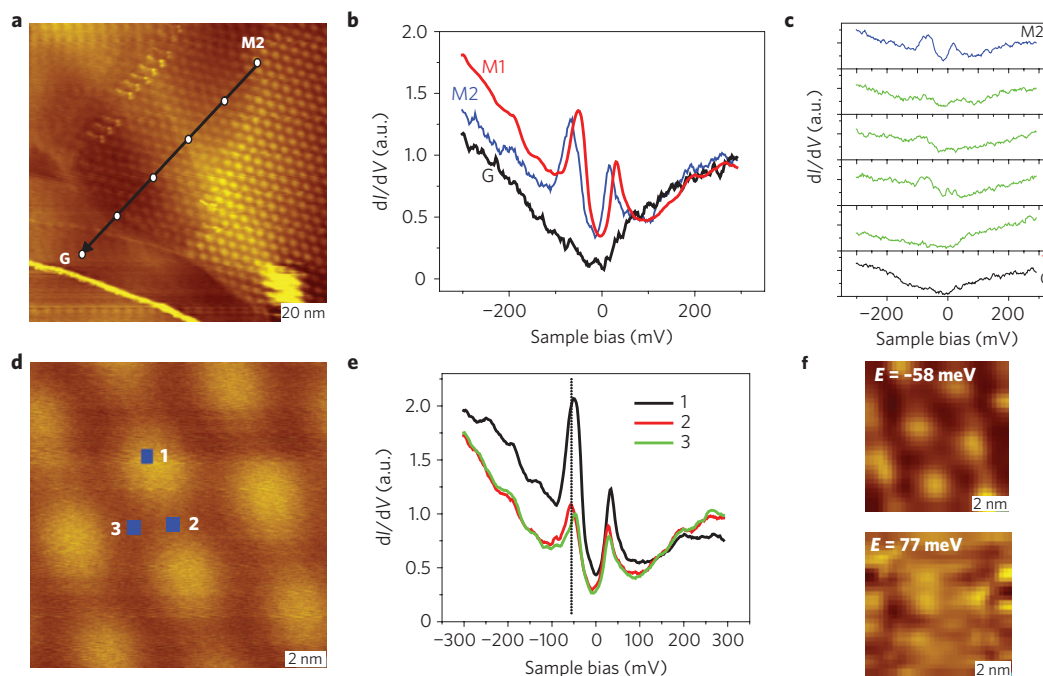


**Figure 2 | STS inside and outside a Moiré pattern with  $\theta = 1.79^\circ$ .** **a**, Topography near the boundary of the pattern. **b**, Tunnelling spectra in the centre of the pattern (M1 in Fig. 1c) and at its edge (M2), showing two sharp peaks flanking the Dirac point with  $\Delta E_{\text{VHS}} \sim 82$  meV. The peaks are absent outside the pattern area (G), where the spectrum is typical of graphite<sup>24</sup>. **c**, Spatial dependence of tunnelling spectra along a line connecting point M2 inside the pattern to point G outside it at positions marked by the white dots in **a**, showing monotonic evolution between the rotated and unrotated regions. Tunnelling current 22 pA, sample bias voltage 300 mV, a.c. bias modulation 5 mV<sub>rms</sub> at 340 Hz. **e**, Comparison of tunnelling spectra on bright and dark regions within the pattern at positions indicated in **d**. Although all spectra show two peaks, the peak heights and degree of asymmetry depend on their position in the pattern. **f**,  $dI/dV$  maps of the region shown in **d**. The top map corresponding to the VHS just below the Fermi energy ( $-58$  meV) shows a strong density modulation, suggesting an imminent Fermi-surface instability. In contrast, the bottom map taken farther from the VHS (77 meV) does not show the modulation.

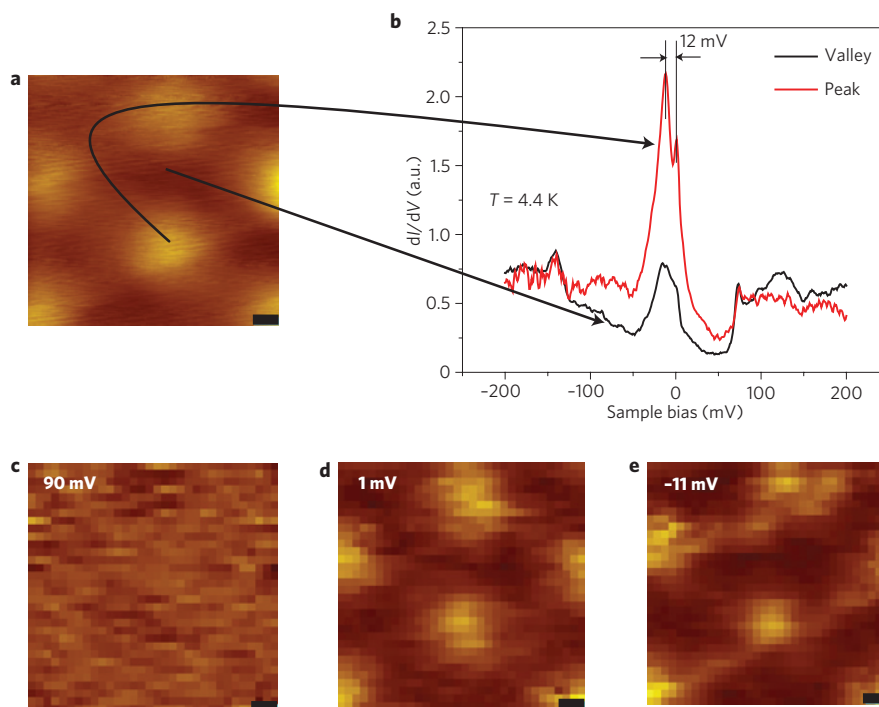


**Figure 3 | Moiré pattern with  $\theta = 1.16^\circ$  on CVD graphene.** **a**, Topography taken at 200 mV and 20 pA, showing a pattern with a superlattice constant of  $12 \pm 0.5$  nm, corresponding to  $\theta \sim 1.16^\circ$ . Scale bar: 2 nm. **b**, Scanning tunnelling spectra taken in bright and dark regions of the pattern. a.c. modulation 1 mV<sub>rms</sub> at 340 Hz. **c–e**,  $dI/dV$  maps of the region shown in **a** at three bias voltages: far from the VHS (90 mV) (**c**), the map is smooth, indicating extended states; and maps at the energies of the VHS, 1 mV (**d**) and  $-11$  mV (**e**), show localized states. Scale bar: 2 nm.

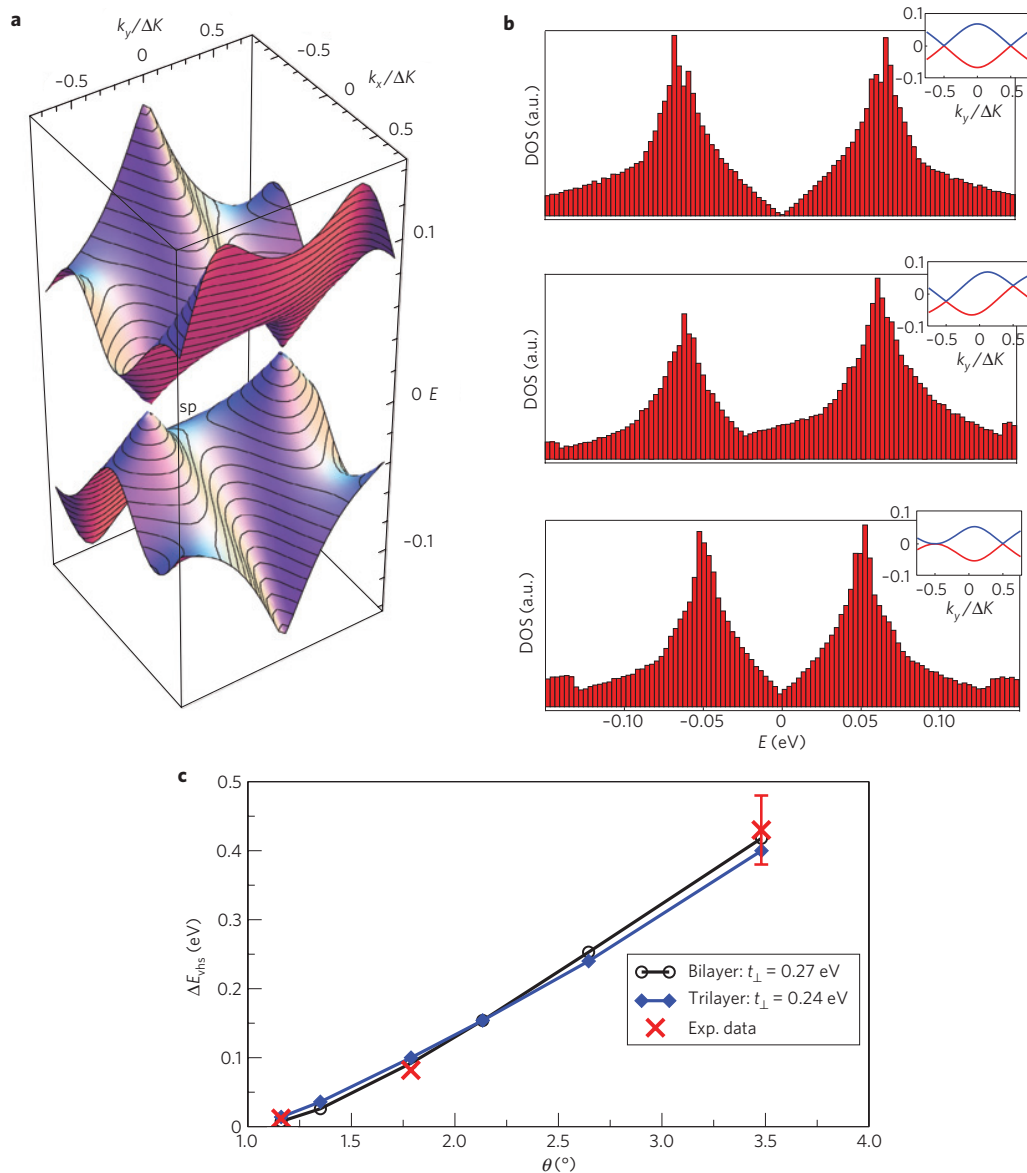


**Figure 4 | Energy separation between VHSs.** **a**, Dispersion of lowest energy states for  $\theta = 1.79^\circ$ ,  $t_{\perp} \approx 0.27$  eV, in a bilayer. A saddle point (marked 'sp') is visible between the two Dirac points in the negative energy band; another one exists in the positive energy band. **b**, Top: DOS of a bilayer with VHSs corresponding to the energy of the saddle points for  $\theta = 1.79^\circ$ ,  $t_{\perp} \approx 0.24$  eV and no interlayer bias; middle: same with interlayer bias  $V_{\text{bias}} = 0.15$  V; bottom: same for a trilayer and no bias. Insets: The band energies along a line joining the two Dirac points for the corresponding layer configurations. **c**, Angle dependence of  $\Delta E_{\text{vhs}}$ . Open circles: bilayer with  $t_{\perp} = 0.27$  eV and  $V_{\text{bias}} = 0$  V; filled diamonds: trilayer  $t_{\perp} = 0.24$  eV,  $V_{\text{bias}} = 0$  V; crosses: experimental data. The error in peak separation was estimated from the peak width at 95% of peak height. The error bars are smaller than the symbols at low angles. Both the bilayer and trilayer fit the results, albeit with slightly different values of  $t_{\perp}$ . For angles  $2^\circ < \theta < 5^\circ$ , the peak separation is roughly described by  $\Delta E_{\text{vhs}} = \hbar v_F \Delta K - 2t_{\perp}^{\theta}$ , but curves upward at smaller angles.

large saddle regions in their band structure<sup>19</sup>, conjectured to be the origin of the CDW instability<sup>5</sup>. However, because the saddle regions and the position of  $E_F$  are determined by the chemical composition, it is difficult to control or predict where instabilities occur. In contrast, in twisted graphene layers, both the position of  $E_F$  and that of the VHSs can be controlled by gating and rotation respectively, providing a powerful toolkit for manipulating electronic phases. To achieve control of  $E_F$ , the graphene sample can be deposited on a non-conducting substrate, or better yet suspended above a gate<sup>20,21</sup>. Although our present experimental set-up did not allow tuning of  $E_F$ , it was possible to find rotated layers in which the VHSs and  $E_F$  were sufficiently close to induce a strong CDW. A method to vary  $\theta$  *in situ* (and thus to control the position of the VHSs) using an AFM was demonstrated in the discovery of superlubricity in

graphite<sup>22</sup>. Superlubricity, which occurs in twisted graphene layers at small rotation angles, was attributed to decoupling of the layers. This led to the assumption that a small twist between layers would decouple them and reveal the electronic structure of an isolated graphene layer<sup>17</sup>. However, counterintuitively, we found that a rotation, however small, markedly affects the band structure and leads to the appearance of VHSs.

The experiments described here demonstrate that in graphene, unlike in any other known material, one can tune the position of the VHSs by controlling the relative angle between layers. As the VHS approaches the Fermi energy, we find a strongly localized CDW corresponding to the wavevector separation between the VHSs. This opens exciting opportunities for inducing and exploring correlated electronic phases in graphene.

Received 3 June 2009; accepted 27 October 2009;  
published online 29 November 2009

## References

1. Van Hove, L. The occurrence of singularities in the elastic frequency distribution of a crystal. *Phys. Rev.* **89**, 1189–1193 (1953).
2. Kohn, W. & Luttinger, J. M. New mechanism for superconductivity. *Phys. Rev. Lett.* **15**, 524–526 (1965).
3. González, J. Konh–Luttinger superconductivity in graphene. *Phys. Rev. B* **78**, 205431 (2008).
4. Fleck, M., Oles, A. M. & Hedin, L. Magnetic phases near the Van Hove singularity in s- and d-band Hubbard models. *Phys. Rev. B* **56**, 3159–3166 (1997).
5. Rice, T. M. & Scott, G. K. New mechanism for a charge-density-wave instability. *Phys. Rev. Lett.* **35**, 120–123 (1975).
6. Castro Neto, A. H., Guinea, F., Peres, N. M. R., Novoselov, K. S. & Geim, A. K. The electronic properties of graphene. *Rev. Mod. Phys.* **81**, 109–162 (2009).
7. Novoselov, K. S. *et al.* Electric field effect in atomically thin carbon films. *Science* **306**, 666–669 (2004).
8. Markiewicz, R. S. Phase separation near the Mott transition in  $\text{La}_{2-x}\text{Sr}_x\text{CuO}_4$ . *J. Phys. Condens. Matter* **2**, 665–676 (1990).
9. Geim, A. K. & Novoselov, K. S. The rise of graphene. *Nature Mater.* **6**, 183–191 (2007).
10. Pong, W. T. & Durkan, C. A review and outlook for an anomaly of scanning tunnelling microscopy (STM): Superlattices on graphite. *J. Phys. D* **38**, R329–R355 (2005).
11. Lopes dos Santos, J. M. B. *et al.* Graphene bilayer with a twist: Electronic structure. *Phys. Rev. Lett.* **99**, 256802 (2007).
12. Tersoff, J. & Hamann, D. R. Theory of the scanning tunnelling microscope. *Phys. Rev. B* **31**, 805–813 (1985).
13. Reina, A. *et al.* Large area, few-layer graphene films on arbitrary substrates by chemical vapour deposition. *Nano Lett.* **9**, 30–35 (2009).
14. Castro Neto, A. H. Charge density wave, superconductivity, and anomalous metallic behaviour in 2D transition metal dichalcogenides. *Phys. Rev. Lett.* **86**, 4382–4385 (2001).
15. Castro, E. V. *et al.* Biased bilayer graphene: Semiconductor with a gap tunable by the electric field effect. *Phys. Rev. Lett.* **99**, 216802 (2007).
16. Li, G., Luican, A. & Andrei, E. Y. Scanning tunnelling spectroscopy of graphene on graphite. *Phys. Rev. Lett.* **102**, 176804 (2009).
17. Miller, D. L. *et al.* Quantization of zero-mass particles in graphene. *Science* **324**, 927–929 (2009).
18. Wilson, J. A., DiSalvo, F. J. & Mahajan, S. Charge-density waves and superlattices in the metallic layered transition metal dichalcogenides. *Adv. Phys.* **24**, 117–201 (1975).
19. Valla, T. *et al.* Quasiparticle spectra, charge-density waves, superconductivity, and electron–phonon coupling in 2H-NbSe<sub>2</sub>. *Phys. Rev. Lett.* **92**, 086401 (2004).
20. Du, X., Skachko, I., Barker, A. & Andrei, E. Y. Approaching ballistic transport in suspended graphene. *Nature Nanotech.* **3**, 491–495 (2008).
21. Bolotin, K. I. *et al.* Ultrahigh electron mobility in suspended graphene. *Solid State Commun.* **146**, 351–355 (2008).
22. Dienwiebel, M. *et al.* Superlubricity of graphite. *Phys. Rev. Lett.* **92**, 126101 (2004).
23. Gwo, S. & Shih, C. K. Site-selective imaging in scanning tunnelling microscopy of graphite: The nature of site asymmetry. *Phys. Rev. B* **47**, 13059–13062 (1993).
24. Mastui, T. *et al.* STS observations of Landau levels at graphite surfaces. *Phys. Rev. Lett.* **94**, 226403 (2007).

## Acknowledgements

E.Y.A. acknowledges D.O.E. support under DE-FG02-99ER45742. E.Y.A. and A.L. acknowledge support from the Lucent-Alcatel foundation and partial NSF support under NSF-DMR-0906711. A.H.C.N. acknowledges partial support of the US Department of Energy under grant DE-FG02-08ER46512. J.M.B.L.S. acknowledges support from FCT under grant PTDC/FIS/64404/2006. A.R. and J.K. acknowledge partial support of NSF DMR 0845358 and the Materials, Structure and Devices centre. A.H.C.N. and J.K. acknowledge support under ONR MURI N00014-09-1-1063. We thank R. Nahir, K. Novoselov and A. Geim for fabricating the CVD graphene membranes.

## Author contributions

G.L. built the STM, collected and analysed data and wrote the paper; A.L. collected and analysed the data; J.M.B.L.S. and A.H.C.N. carried out the theoretical work and wrote the paper; A.R. and J.K. carried out the CVD growth of graphene; E.Y.A. directed the project, analysed the data and wrote the paper.

## Additional information

The authors declare no competing financial interests. Supplementary information accompanies this paper on [www.nature.com/naturephysics](http://www.nature.com/naturephysics). Reprints and permissions information is available online at <http://npg.nature.com/reprintsandpermissions>. Correspondence and requests for materials should be addressed to E.Y.A.